Multiple Adaptive Model Predictive Controllers for Frequency Regulation in Wind Farms

Haixin Wang, *Member*, *IEEE*, Zihao Yang, Zhe Chen, *Fellow*, *IEEE*, Jun Liang, *Senior Member*, *IEEE*, Gen Li, *Member*, *IEEE*, Junyou Yang, and Shiyan Hu, *Senior Member*, *IEEE*

***Abstract*—Frequent and inadequate power regulation could significantly impact the main shaft mechanical load and the fatigue of wind turbines, which imposes a stringent requirement to perform frequency regulation. However, the existing work on frequency regulation mainly uses torque compensation to improve the frequency response, while few of them consider the mechanical fatigue of the main shaft caused by torque compensation of the frequency controller. In this paper, the mechanical fatigue of the main shaft can be mitigated in all of the speed sections thanks to the proposed frequency regulation controllers. Precisely, a multiple adaptive model predictive controller (MAMPC), which seamlessly integrates the multiple model predictive control (MMPC) and the real-time AutoRegressive with eXogenous inputs (ARX) model, is proposed. It nicely handles the rate of change in compensation torque to mitigate the mechanical load on the shaft in all of the speed sections. The effectiveness of our method is verified through extensive simulations. With the proposed method, the minimum frequency deviation can be reduced, and the number of fatigue cycles of the main shaft can be extended.**

***Index Terms*—Multiple adaptive model predictive controllers, wind farm, frequency regulation, deloading torque method, torque compensation control.**

NOMENCLATURE

Power System Model

$f_{on,dev}$	Onshore frequency deviation of the AC grid.
M	Inertia constant of the power system.
D	Damping coefficient of the power system.
P_{dev}	Power deviation of the power system.
P_{wf}	Wind farm output.
P_{dc}	DC capacitor output of the HVDC.
P_l	Load power.
P_g	AC grid output.
R	Droop coefficient of the SG droop controller.
K_I	Integral coefficient of the SG droop controller.
T_d	Mechanical time constants of the SG turbine.
T_g	Mechanical time constants of the SG governor.
$P_{g,ref}$	Input of the SG governor.
$P_{g,gov,ref}$	Output of the SG governor.

GSC Model of HVDC

i_{gabc}	Three-phase output current.
ω_{on}	AC grid angular frequency.
L_{on}	GSC filter inductance.
V_{dc}	DC-link voltage of GSC.
$i_{d,g}$, $i_{q,g}$	d-q axis currents of GSC.
$i_{gd,ref}$, $i_{gq,ref}$	d-q axis current references of GSC.
$v_{gd,ref}$, $v_{gq,ref}$	d-q axis output voltage references of GSC.
k_{fV}	Droop coefficient f_{on} vs. V_{dc} droop controller.
C	Equivalent capacitance of DC-link capacitor.

WFC Model of HVDC

$V_{wdq,ref}$	Voltage references of the outer loop of WFC.
V_{wabc}, i_{wabc}	Three-phase voltage and current of OWF.
$i_{wd,ref}$, $i_{wq,ref}$	Current references of the inner loop of WFC.
i_{wd}, i_{wq}	d-q axis currents of WFC.
L_{off}	Filter inductance of WFC.
ω_{off}	Angular frequency of OWF.
$v_{wd,ref}$, $v_{wq,ref}$	Output voltage references of WFC.
θ_{off}	Phase angle of WFC.
f_{off}	Offshore frequency of WFC.
k_{Vf}	Droop coefficient V_{dc} vs. f_{off} droop controller.

WTG Model

T_m	Mechanical torque.
ρ	Density of air.
C_p	Wind power utilization coefficient.
λ	Tip speed ratio.
β	Pitch angle.
A_r	The swept area of wind turbine.
V_w	Wind speed.
ω_r	Angular speed.
P_e	Output power of WTG
H	Inertia constant.
$T_{e,tra}$	Electromagnetic torque with traditional method.
k_{opt}	Optimal factor.
$T_{e,\mathrm{nom}}$	Nominal electric magnetic torque.
ω_1	Cut-in angular speed.
ω_2	The initial angular speed of transition section.
$\omega_{r,\mathrm{nom}}$	Nominal angular speed.
$\omega_{r,\max}$, $\omega_{\min}$	The minimum and minimum angular speeds.
$P_{e,\mathrm{nom}}$	Nominal output power.
T_e	Electromagnetic torque.
$T_{e,com}$	Torque compensation component.
k_f	Deloading factor.
$\omega_{r,ref}$	Angular speed reference.
β_{ref}	Pitch angle reference.
τ_β	Mechanical time constant of pitch servo.
R_w	Blade radius.
$V_{w,av}$	Average wind speed.
N	The number of fatigue cycles of main shaft.
S_u	Yield limit of the main shaft.

This work was supported by the Liaoning Province Doctoral Research Start-up Funding under Grant 2020-BS-141. *(Corresponding author: Junyou Yang)*

H. Wang, Z. Yang and J. Yang are with the School of Electrical Engineering, Shenyang University of Technology, Shen Yang, 110870, China (email: haixinwang@sut.edu.cn; yangzihaotod0131@163.com; junyouyang@sut.edu.cn).

Z. Chen is with AAU Energy, Aalborg University, Alborg 9220, Denmark (e-mail: zch@energy.aau.dk).

J. Liang is with the School of Engineering, Cardiff University, Cardiff CF24 3AA, U.K. (e-mail: liangj1@cardiff.ac.uk).

G. Li is with the Electric Energy Group, Department of Engineering Technology and Didactics, Technical University of Denmark (DTU), 2750 Ballerup, Denmark (email: genli@dtu.dk).

S. Hu is with the School of Electronics and Computer Science, University of Southampton, Southampton, SO17 1BJ, U.K. (e-mail: s.hu@soton.ac.uk).

$\tau_{\max}$, $\tau_{\min}$	The maximum and minimum shear stress.
$T_{e,\max}$, $T_{e,\min}$	The maximum and minimum torques.
W_T	Torsional section modulus of main shaft.
K_{droop}	Droop coefficient of variable droop controller.

Model Predictive Controller

p	Prediction cycles of MPC.
ε_1, ε_2, ε_3	Weight coefficients of objective function.
$\hat{\boldsymbol{Y}}$	Predictive output matrices.
$\boldsymbol{S}$, $\boldsymbol{L}$	Coefficients matrices.
$\boldsymbol{X}$, $\boldsymbol{U}$	State variable and input matrices.
$\boldsymbol{W}$	Desired output matrices.
$\boldsymbol{D}(u)$	Derivative matrices of input.
$\boldsymbol{Q}$, $\boldsymbol{R}$, $\boldsymbol{D}$	Positive definite weighting matrices.

I. Introduction

With increasing penetration of wind farm (WF), the decreased rotational inertia of power systems could induce power imbalance and impact their frequency response capability. Wind power has the potential to provide ancillary frequency regulation services [1]. However, insufficient design may influence the reliability and lifetime of a component of a wind turbine generator (WTG) [2]-[3]. Frequent regulation of shaft torque will impact the main shaft fatigue life when the WTG participates in frequency regulation, which cannot be ignored [4]. It is highly desirable to develop frequency regulation methods for WTG.

WTG needs power reserve to regulate output power for frequency suppression. Without external storage devices, WTG responds to frequency variation through three approaches: ***1)*** Inertia control [5]. WTG normally runs in the maximum power point tracking (MPPT) mode. WTG can release part of their kinetic energy so as to temporarily increase the output power. However, due to the rapid change of WTG speed, severe instability of WTG and the second drop in grid frequency can be easily induced [6]. ***2)*** Pitch control [7]-[8]. One can reserve a certain spare angle for the pitch system such that the WTG can obtain external power reserve. However, frequent action of pitch actuator may lead to mechanical wear. WTG cannot fully rely on the pitch system to regulate frequency due to its delay characteristic [9]. ***3)*** Deloading control [10]-[11]. In this case, WTG will not operate in the MPPT mode, and the power reserve can be achieved by over-speeding control. Among the above methods, the deloading method is most effective due to their simple application and fast response to frequency variations [12]. The deloading method refers to decrease electromagnetic torque to make WTG obtain more energy for frequency regulation. Thus, the deloading method is considered in this paper.

The main target of frequency regulation is to compensate for the output power by the supplementary control for WTGs [13] and the most popular strategy is the variable droop control [14]-[15]. A droop frequency control technique is developed to improve frequency stability and autonomous power sharing in [16]. In addition, the work in [17] adjusts a real-time variable droop coefficient considering the optimization of WTG rotor kinetic energy. In terms of offshore WF (OWF), voltage source converter based high voltage DC (VSC-HVDC) has been recognized as an effective alternative to transmitting wind power to AC grids [18]. Two droop controllers are developed in the grid-side converter (GSC) and wind-farm converter (WFC) of the HVDC system to support grid frequency [19]. A low-order response model is proposed for OWFs and VSC-HVDC to participate in frequency regulation [20]. Literatures [21]-[23] analyze the frequency support characteristics of VSC-HVDC, and propose a dead-band controller for the coordination of frequency support.

Moreover, when the WTGs are performing the frequency regulation, the controllers regulate the electromagnetic torque to change the output power. Frequent torque changes may exacerbate the fatigue of the main shaft of WTG [24]. Reference [25] studies the mechanical resonance of frequency-regulating WTGs. [26] points out frequency regulation will worsen the torque vibration of the transmission system of WTGs. In [27], an electromagnetic coupler between the shaft and the generator has been added to solve the coupling effect between the frequency regulation and the mechanical load of WTGs, which will increase the cost and the complexity of the control strategy. Fatigue load effects of WTG under different deloading strategies are analyzed in [28]. However, this fatigue is not caused by frequency regulation. Few of the open literature consider the main shaft mechanical fatigue caused by torque compensation of the frequency regulation controller, and no specific solution is provided.

To suppress the rapid variation of rotor speed induced by the release of kinetic energy, literatures [29]-[30] introduce the speed limit and torque limit in the control loop. However, these fixed limits are not sufficient to mitigate of mechanical load of main shaft effectively. Furthermore, model predictive control (MPC) with strong dynamic characteristics has been applied in a multi-energy integrated system to regulate frequency [31], but the existing MPC based frequency regulation techniques are lack of consideration of main shaft mechanical fatigue and torque characteristics in different speed sections of WTG.

Literatures [14]-[17] develop variable droop controllers which only consider the frequency deviation and literatures [18]-[23] focus on the high-level coordination of wind farms. However, WF owners need to consider the main shaft mechanical load of wind turbines. In the literature, the only such works are [29] and [30]. However, the main shaft mechanical load might still be significant even after their mechanical load mitigation process due to their adapted stationary limitation ranges in the torque control loop.

MPC has the strong dynamic adjustment ability for disturbances of wind speed and load in the process of frequency regulation, and it can facilitate to optimize the mechanical load by the inherent decoupling characteristic of the rolling function. The growth of the available computational capability, together with some recent research works [31]-[33], has shown the potential of MPC strategies in WTG applications for frequency regulation. This motivates this work to develop an MPC based technique. However, the existing MPCs are lack of prediction of operation condition and consideration of corresponding torque control in all speed sections. Thus, we proposed the

multiple adaptive model predictive controllers (MAMPC) to limit the rate of change of the torque compensation to mitigate the main shaft mechanical fatigue of the WTG.

As aforementioned, the existing frequency regulation approaches cannot handle the issues such as mitigating the main shaft mechanical load caused by the torque compensation, predicting the operation condition of WTG in all speed sections, and enhancing the anti-disturbance ability. This paper aims to tackle these issues. Our contributions are as follows.

- To the best of our knowledge, this is the first work mitigating the main shaft mechanical fatigue caused by the torque compensation using frequency regulation controllers which restrict torque compensation in all speed sections.
- A multiple adaptive model predictive control (MAMPC) technique, which integrates the multiple model predictive control (MMPC) and the real-time AutoRegressive with eXogenous inputs (ARX) model, is proposed to mitigate the mechanical load, through predicting the real-time operation condition and performing the corresponding torque control.
- Comparing with the state-of-the-art techniques of MPPT, variable droop and MMPC, the minimum frequency deviation with the proposed method can be reduced by 0.1 Hz, 0.05 Hz and 0.03 Hz, in the case of a 0.2 p.u. load rise.

II. System Modeling

In this paper, an HVDC offshore wind system is studied. The wind power is transmitted via transformer and high voltage DC (HVDC) into AC grid. The simulation model in MATLAB Simulink is shown in Fig. 1. (Note: In Fig. 1, we use '_' to replace the mark ',' in the names of the variables considering the restrictive definition of variables in MATLAB.) It is clear from Fig. 1 that our main contribution is to develop a frequency regulation method in WTG for the main shaft mechanical load mitigation, while the other parts follow the existing literature. HVDC consists of a wind-farm converter (WFC) and a grid-side converter (GSC). We model the AC grid as a synchronous generator (SG) model. The detailed modeling is as follows.

A. SG Model

The onshore frequency deviation $f_{on,dev}$ of the AC grid is obtained by the frequency dynamic model $H_g(s)$ [33]. The input variable of the model is the power deviation P_{dev} of the power system, which is the sum of the wind farm output P_{wf}, DC capacitor output P_{dc} of the HVDC, the load power P_l and the AC grid output P_g. The AC grid frequency is regulated by the droop controller and the integrator of the SG. Delay characteristics caused by governor and turbine are modeled.

B. GSC Model

Fig. 1 shows the structure of the outer and inner loop controllers of the GSC. The GSC uses a vector control strategy in which the d-axis current $i_{d,g}$ stabilizes the DC-link voltage V_{dc} and the q-axis current $i_{q,g}$ controls reactive power. The outer loop uses PI controllers to compute the d-axis current reference $i_{gd,ref}$, which is sent to the inner loop. The q-axis current reference $i_{gq,ref}$ is set to zero. To suppress the variation of grid frequency f_{on}, a f_{on} vs. V_{dc} droop control method is applied in the GSC. The variation of the AC grid frequency is linked with the DC-link voltage through the droop control. The GSC will provide frequency response through regulating the DC-link voltage when the frequency changes. For instance, a 10% droop or regulation means that a 0.5 Hz frequency deviation will cause a 5% change of the DC-link voltage. The DC-link capacitor output P_{dc} of HVDC is modeled as (1) [22].

$$P_{dc} = V_{dc} C \frac{dV_{dc}}{dt}, \tag{1}$$

C. WFC model

The main roles of the WFC are to transmit OWF power to the HVDC system and establish a stable voltage with constant magnitude and frequency. The WFC also uses outer and inner loop controllers. Voltage references $V_{wdq,ref}$ of the outer loop are constant. The generated current references $i_{wd,ref}$ and $i_{wq,ref}$ are sent to the inner loop. The phase angle of the GSC is obtained from the onshore AC grid based on the phase-locked loop. The phase angle θ_{off} of the WFC is generated by its own frequency oscillator. Thus, the WFC can produce its self-designed offshore frequency f_{off} according to system requirements. To

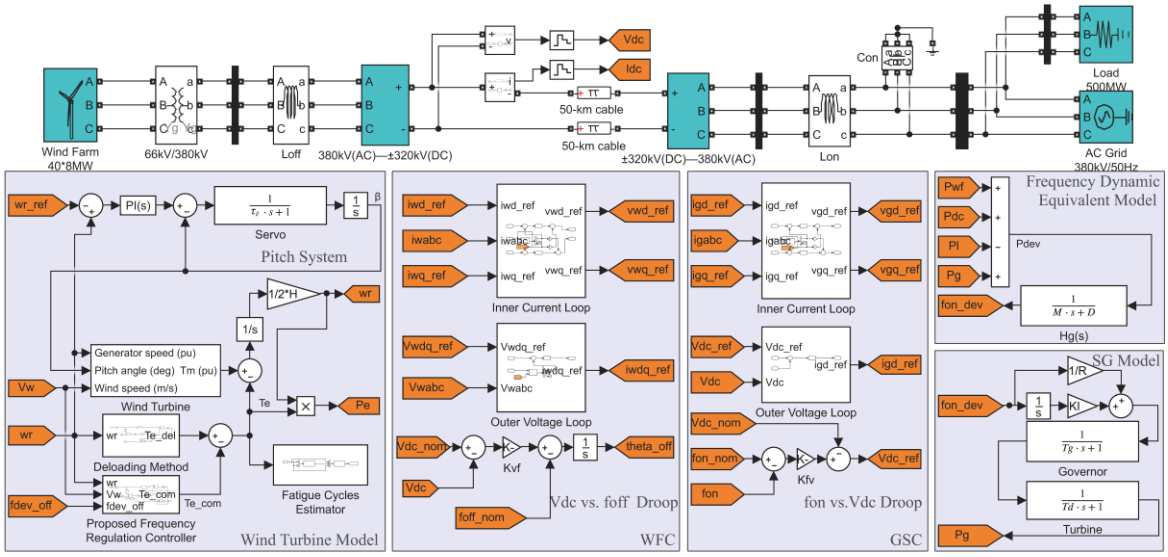

Fig. 1. Overall system structure.

provide frequency information of the onshore AC grid to the WTG, a V_{dc} vs. f_{off} droop control method is adopted in the offshore WFC. The frequency variation of the OWF is linked with the DC-link voltage through this droop control.

D. WTG Model

The wind turbines as shown in Fig. 1 are modeled by (2) [33].

$$T_m = 0.5\rho C_p(\lambda,\beta)A_r V_w^3/\omega_r, \tag{2}$$

The electromagnetic torque reference of WTG is calculated by the following traditional method [33]:

$$T_{e,tra} = \begin{cases} k_{opt}\omega_r^2, & \omega_1 < \omega_r \le \omega_2 \text{ (3a)} \\ \dfrac{T_{e,\text{nom}} - k_{opt}\omega_1^2}{\omega_{r,\text{nom}} - \omega_1}(\omega_r - \omega_{r,\text{nom}}) + T_{e,\text{nom}}, & \omega_2 < \omega_r < \omega_{r,\text{nom}} \text{ (3b)} \\ \dfrac{P_{e,\text{nom}}}{\omega_r}, & \omega_{r,\text{nom}} \le \omega_r < \omega_{r,\max} \text{ (3c)} \end{cases} \tag{3}$$

There are three speed sections: section 1($\omega_1<\omega_r<\omega_2$), section 2($\omega_2<\omega_r<\omega_{r,\text{nom}}$) and section 3($\omega_{r,\text{nom}}<\omega_r<\omega_{r,\max}$). WTG participates in frequency regulation by three ways: inertial control, pitch control and deloading control. We choose deloading control method to gain more power reserve for frequency regulation. The electromagnetic torque T_e is calculated by (4).

$$T_e = \underbrace{k_f T_{tra}}_{\text{Deloading torque } T_{e,del}} + \underbrace{T_{e,com}}_{\text{Torque compensation}}, \tag{4}$$

The torque compensation $T_{e,com}$ is generated by frequency regulation controller to adjust output power. The deloading factor k_f needs to be selected based on actual requirements. If k_f is too large, fewer power reserve will cause less contribution to supporting frequency response. If k_f is too small, economic benefits will be reduced for wind farm owners. Refer to [33] for further details. We select k_f as 0.9. In the three speed sections, the deloaded WTG has different torque algorithms, which will be considered in the prediction model design of MPC. In speed section 3, the pitch system stabilizes the rotor speed at its reference $\omega_{r,ref}$ to avoid overspeed in Fig. 1.

III. The Proposed Frequency Regulation Method

Compared with cases without involving the frequency regulation, the change of torque compensation has an influence on the shaft mechanical fatigue. MPC strategies are popular due to their inherent dynamic characteristics and flexible control capability [34]-[35]. MPC can mitigate the mechanical fatigue of WTG using the rolling optimization function. The other advantage of MPC is that it can predict the grid frequency deviation, which is beneficial to enhance the anti-disturbance ability of wind speed and load.

To mitigate the main shaft mechanical load and enhance the frequency response performance of WFs, a MAMPC is proposed for individual WTG. Note that there are MMPC technique [36] and adaptive MPC (AMPC) technique [37] designed for the similar purposes in the literature. However, none of them is suitable in our context. MMPC can achieve switching controllers in corresponding multiple speed sections, but its operation range around the operating points is limited. AMPC has the ability to estimate real-time parameters, but it has only one MPC, so it cannot tackle the nonlinear control problem owning in all of the speed sections. Thus, it is highly necessary to develop a new technique to facilitate the excellent torque compensation in all of the speed sections. Such a technique is developed in this paper, and we call it multiple adaptive model predictive controllers (MAMPC). In fact, our technique can be viewed as a seamless integration of the merits of MMPC and AMPC.

The MAMPC predicts operating conditions considering wind speed, speed sections, frequency deviation, and provides torque compensation. As a popular control method, MPC consists of predictive control, feedback correction and rolling optimization. Predictive control is based on the discrete linearized state-space model of controlled objects [32]. Assume that the WF has n wind turbines, where the subscript i denotes the i th WTG (i=1, 2, 3, …n). The individual wind turbine has the same control strategies. The equally proportional distribution method is used to distribute torque compensation to individual wind turbine according to the corresponding operating condition.

A. Frequency Analysis and Dead-band

Due to the isolation of the HVDC system and the long distance, an OWF may not obtain the information of frequency variation in an onshore AC grid directly. Hence, local measurements of each system (GSC, WFC and WTGs) are utilized to transmit the frequency variation in onshore AC grid to each WTG. Thanks to the droop controls shown in Fig. 1, the frequency is linked with the DC-link voltage. GSC measures the onshore frequency deviation and shifts it to the DC-link voltage. WFC detects the DC-link voltage variation and translates it into the OWF frequency. All systems are controlled to provide frequency response. If the frequency responses of the GSC and WFC are accurate and instant, the OWF can simultaneously follow the onshore frequency [38].

Torque regulation may affect the mechanical fatigue of wind turbines which are unacceptable to wind farm owners. To avoid unnecessary frequent adjustments and noise, a dead-band f_{db} is induced whose scheme diagram in Fig. 2. The droop loop will be activated when the frequency deviation exceeds the dead-band. Meanwhile, to avoid the sudden change of the torque compensation, f_{db} will reduce the frequency deviation.

B. Linearization Models

Due to the limited contribution of the DC-link capacitor for frequency regulation, the P_{dc} in the linearization process is ignored. Since the rotational speed operation range of WTG includes different control methods, three linearization plants are considered based on the rotational speed sections. According to (3a), the discrete linearized state-space model at a stable operating point of section 1 is obtained in (5).

$$\begin{cases} x(k) = Ax(k-1) + Bu(k-1) \\ y(k) = Cx(k-1) \end{cases} \tag{5}$$

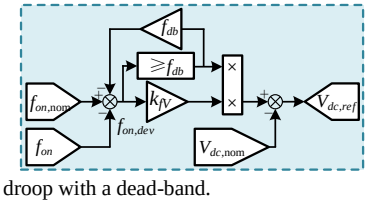

Fig. 2. f_{on} vs. V_{dc} droop with a dead-band.

where state variables are x=[$\Delta P_{g,ref}$ $\Delta f_{on,dev}$ $\Delta P_{g,gov,ref}$ ΔP_g $\Delta\omega_{ri}$], u=[ΔV_w $\Delta T_{e,comi}$ ΔP_{dev}] the input variables, y=$\Delta f_{on,dev}$ the output variable, A the state matric, B the input matric and C the output matric. In speed section 2, the structure of the discrete linearized state-space model based on (3b) at a stable operating point is the same as the model in section 1, and the parameters of system matrices are different. In section 3, ω_{ri} will remain constant due to the pitch control in steady-state conditions. The state variables are changed to x=[$\Delta P_{g,ref}$ $\Delta f_{on,dev}$ $\Delta P_{g,gov,ref}$ ΔP_g] based on (3c).

C. Multiple Model Predictive Controllers

When the control variables $\Delta T_{e,comi}$ in the future p prediction cycles are different, according to Eq. (5), the predicted value of the system state is expressed by (6).

$$\begin{cases} x_m(k+1|k) = Ax(k) + Bu(k) \\ x_m(k+2|k) = Ax_m(k+1) + Bu(k+1) \\ \vdots \\ x_m(k+p|k) = Ax_m(k+p-1) + Bu(k+p-1) \end{cases} \tag{6}$$

The controlled object is optimized within p prediction cycles after instant k. To accurately approximate the prediction value $\Delta f_{on,dev,m}(k+h|k)$ to the reference value $\Delta f_{on,dev,ref}(k+h)$, and to avoid severe changes in control variables and the shaft fatigue within m control cycles after instant k, the following objective function is proposed:

$$\min J(k) = \sum_{h}^{p} \varepsilon_1 \left[\Delta f_{on,dev,m}(k+h \mid k) - \Delta f_{on,dev,ref}(k+h) \right]^2 + \sum_{j}^{m} \varepsilon_2 \left[\Delta T_{e,comi}(k+j-1) \right]^2 + \sum_{j}^{m} \varepsilon_3 \left[\frac{d\Delta T_{e,comi}(k+j-1)}{dt} \right]^2 \tag{7}$$

The weight coefficients (ε_1, ε_2 and ε_3) are sensitive to the controller output. ε_1 indicates the expectation of the frequency stability. A large ε_1 will lead to a large torque compensation which means that the controller is aggressive. ε_2 affects the gain of the controller which will restrict the contribution for frequency stability. ε_3 determines the rate of change in torque compensation which will affect the main shaft mechanical load and fatigue. Based on the optimization of each function, the proposed controller can not only enhance the performance of frequency regulation, but also can mitigate shaft fatigue. In this paper, to illustrate our approach we select ε_1, ε_2 and ε_3 as 1, 0.06 and 1, respectively. However, our approach is not limited to this set of parameters. The compact form of (7) can be written as

$$\min J = (\hat{\boldsymbol{Y}} - \boldsymbol{W})^{\mathrm{T}} \boldsymbol{Q} (\hat{\boldsymbol{Y}} - \boldsymbol{W}) + \boldsymbol{U}^{\mathrm{T}} \boldsymbol{R} \boldsymbol{U} + \boldsymbol{D}(u)^{\mathrm{T}} \boldsymbol{G} \boldsymbol{D}(u) \tag{8}$$

where $\hat{\boldsymbol{Y}}$ is the predictive output matrices, and can be written as ($\boldsymbol{SX}$+$\boldsymbol{LU}$), $\boldsymbol{S}$ and $\boldsymbol{L}$ are matrices of coefficients, $\boldsymbol{X}$ and $\boldsymbol{U}$ are state variable and input matrices, $\boldsymbol{W}$ is desired output matrices, and $\boldsymbol{D}(u)$ is derivative matrices of input. $\boldsymbol{Q}$, $\boldsymbol{R}$, $\boldsymbol{D}$ are positive definite weighting matrices. Since $\boldsymbol{U}$ is not included in the term $\boldsymbol{SX}$, equation (8) can be written as (9). One can then solve $\partial J / \partial u = 0$ to obtain $u(k)$.

$$\min J = (\boldsymbol{S} - \boldsymbol{W})^{\mathrm{T}} \boldsymbol{Q} \boldsymbol{L} \boldsymbol{U} + \boldsymbol{U}^{\mathrm{T}} \boldsymbol{L}^{\mathrm{T}} \boldsymbol{Q} (\boldsymbol{S} - \boldsymbol{W}) + \boldsymbol{U}^{\mathrm{T}} (\boldsymbol{L}^{\mathrm{T}} \boldsymbol{Q} \boldsymbol{L} \boldsymbol{R}) \boldsymbol{U} + \boldsymbol{D}(u)^{\mathrm{T}} \boldsymbol{G} \boldsymbol{D}(u) \tag{9}$$

The MPC design structure is shown in Fig. 3. The MPC has three inputs and one output. Wind speed and frequency deviation are considered in the controller for obtaining the

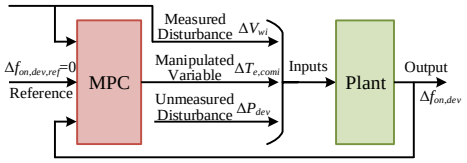

Fig. 3. MPC design structure.

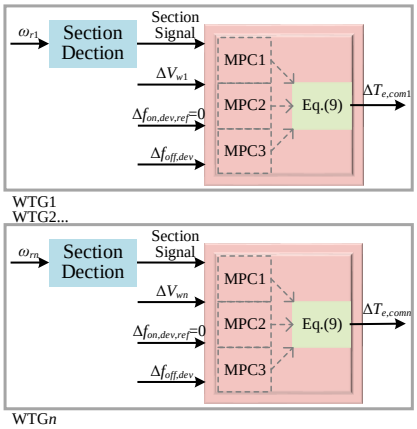

Fig. 4. MMPC structure in WTGs.

operation information of WTGs and power system. The plant is a linearization model at a stable operating point of controlled objects. The MPC can be realized and tuned in MATLAB MPC designer app (R2018a version). The closed-loop performance and state estimation performance of MPC are tuned. For closed-loop performance, increasing the manipulated variable rate weight of the controller and decreasing the output variable weight will produce a more robust controller. Conversely, it will lead to tighter control of outputs and more aggressive control moves. Similarly, for state estimation performance, increasing unmeasured disturbance weight will lead to more aggressive unmeasured disturbance rejection, and vice versa. Thus, one can tune the parameters to decide the balance performances according to the specific model and demands. The operation condition and regulation capability of the WTG are different in the different speed sections. Thus, according to the standard MPC structure, multiple MPCs (MPC1-3) are developed based on different linearization models in the three speed sections. When rotational speed is in section 1, section 2 or section 3, MPC 1, MPC 2 or MPC 3 will be enabled, respectively. The MMPC structure in WTGs is shown in Fig. 4. The MMPC is applied to individual WTG for frequency regulation. The rotational speed is utilized to detect the speed sections to select the proper MPCs.

D. Multiple Adaptive Model Predictive Controllers

MMPC is counting on switching controllers for different operating sections to solve nonlinear control problems using operating points and linear control techniques. If one operating point in each speed section is used to obtain the linearization model for the MMPC (V_{w0}=10, 11, 13m/s) by Eq. (5), it is not sufficient to consider only three stable operating points for the whole operation range of WTG owning to the varying inputs and disturbances with varying time. More operation points need to be considered. When a large number of stable operating points are used, the computational overhead is significant. Thus, the MAMPC, which seamlessly integrates MMPC [31] and the real-time ARX model [34], is proposed in this paper. It can

facilitate the excellent torque compensation in all of the speed section. Recall that ARX is an essential feature for AMPC [32]. However, AMPC itself is not suitable for our context. If one would use AMPC alone, then there would be only one MPC in Fig. 5, which cannot handle all of the speed sections. Thus, our MAMPC can be viewed as a seamless integration of MMPC and AMPC.

For a multiple-input single-output system, ARX model can estimate the real-time model parameters for more different operation points [39]. Though the system parameters are unknown, the ARX model can use real-time plant data to estimate the model parameters according to the model orders for a linear-time-varying (LTV) model. Inputs of the ARX model are the input and output variables of the linearization models. Since ΔP_{dev} is an unmeasurable input, the ARX model is described in (10).

$$A(z)\Delta f_{off,dev}(k) = B(z)\begin{bmatrix}\Delta V_{wi}(k-n_k)\\ \Delta T_{e,comi}(k-n_k)\end{bmatrix} + e(k), \tag{10}$$

where z is the time-shift operator, n_k is the delay and $e(k)$ is the error, $A(z)$ and $B(z)$ are polynomials. The Kalman filter is used as the estimation method. Following [32], the outputs of the ARX model are the polynomial model coefficients, and one can then convert the model coefficients of ARX to state-space matrices A_i, B_i, C_i. The MPC is designed and implemented based on this state-space matrices. Since the rotor speed is stabilized by pitch control system at its nominal speed in speed section 3, the state variables and state-space matrices are different from the other two speed sections. Thus, two ARX models corresponding to different speed sections are established as shown in (11) and (12), respectively. Their orders of $A(z)$ and $B(z)$ are selected by Akaike's Information Criterion. Therefore, the real-time plant parameters of WTG are estimated by two ARX models automatically. When the speed section is detected, the parameters are estimated by a single corresponding ARX model.

$$\begin{cases} A(z) = 1 + a_1 z^{-1} + a_2 z^{-2} + a_3 z^{-3} + a_4 z^{-4} + a_5 z^{-5} \\ B(z) = \begin{bmatrix} b_{11} + b_{12} z^{-1} + b_{13} z^{-2} + b_{14} z^{-3} + b_{15} z^{-4} + b_{16} z^{-5} \\ b_{12} + b_{22} z^{-1} + b_{23} z^{-2} + b_{24} z^{-3} + b_{25} z^{-4} + b_{26} z^{-5} \\ b_{13} + b_{32} z^{-1} + b_{33} z^{-2} + b_{34} z^{-3} + b_{35} z^{-4} + b_{36} z^{-5} \end{bmatrix} \end{cases} \text{(Sections 1, 2)} \tag{11}$$

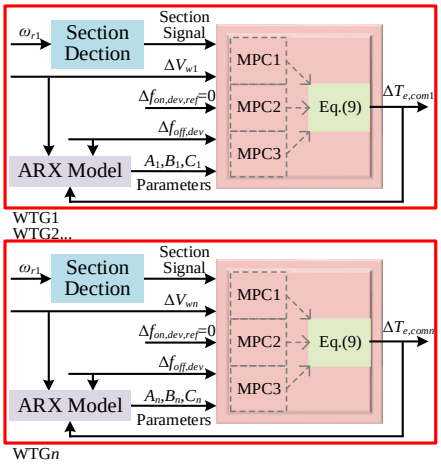

Fig. 5. MAMPC structure in WTGs.

$$\begin{cases} A(z) = 1 + a_1 z^{-1} + a_2 z^{-2} + a_3 z^{-3} + a_4 z^{-4} \\ B(z) = \begin{bmatrix} b_{11} + b_{12} z^{-1} + b_{13} z^{-2} + b_{14} z^{-3} + b_{15} z^{-4} \\ b_{12} + b_{22} z^{-1} + b_{23} z^{-2} + b_{24} z^{-3} + b_{25} z^{-4} \\ b_{13} + b_{32} z^{-1} + b_{33} z^{-2} + b_{34} z^{-3} + b_{35} z^{-4} \end{bmatrix} \end{cases} \text{(Section 3)}. \tag{12}$$

Fig. 5 shows the MAMPC structure in WTGs. The predicted parameters are the input of MAMPC. The ARX model are used by the inactive controllers to perform state estimation which can provide smooth transfer between controllers. The proposed method is illustrated in the flowchart in Fig. 6.

When the change in wind speed is severe, there could be significant disturbances to the ARX model performance. Thus, to mitigate the impact on the input ΔV_{wi}, a linear filter developed in [40] is used in this paper.

$$H_{filter}(s) = \frac{0.99 + 4.79ds}{1 + 7.35ds + 7.68(ds)^2}, \tag{13}$$

where $d=R_w/V_{w,av}$.

E. Fatigue Cycles Estimation of the Main Shaft

Since the torque compensation generated by frequency regulation controller could worsen the mechanical fatigue in the torsion direction of the drive chain, we assess the mechanical fatigue of the main shaft connected to the generator. During the process of regulating frequency, the proposed MAMPC, as a frequency support controller, limits the rate of change of the torque compensation to mitigate the mechanical load of the

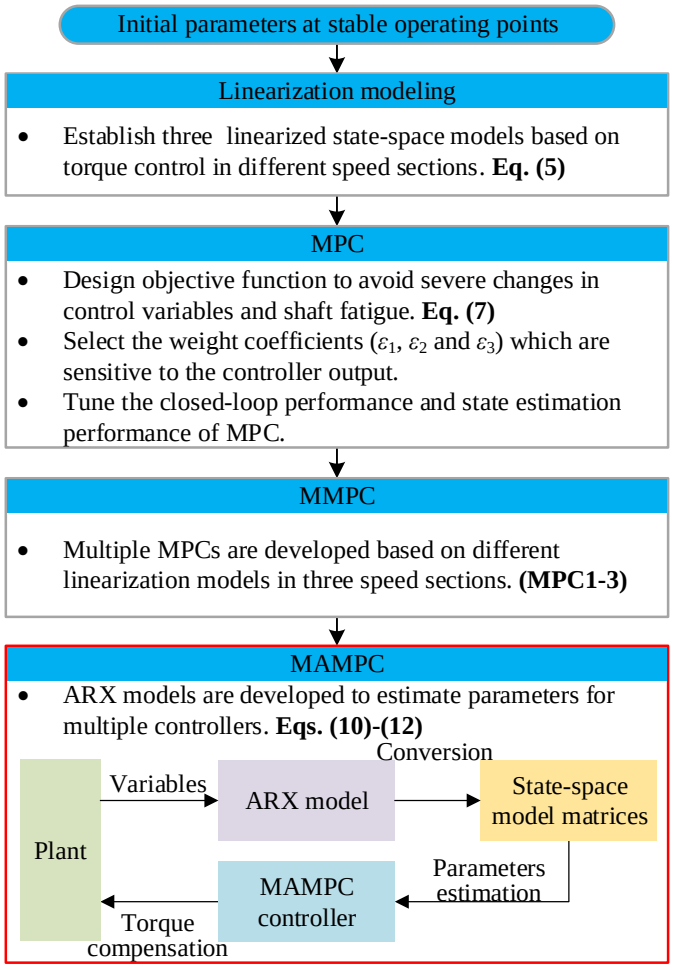

Fig. 6. The detail flowchart of the proposed method.

TABLE I
SIMULATION PARAMETERS

System	Parameters	Values
Onshore AC grid	Nominal voltage	380 kV
	Nominal frequency $f_{on,\mathrm{nom}}$	50 Hz
	Load capacity	500 MW
	Inertia constant M	10
	Damping coefficient D	0.8
HVDC system	Nominal voltage	±320 kV
	Transmission line resistance	0.01273Ω/km
	Transmission line capacitance	0.01274uF/km
	Transmission line reactance	0.9337mH/km
Offshore wind farm	Nominal power	320 MW
	Quantities of WTGs	40
	WTG nominal power	8 MW
	Rated wind speed	12 m/s
	Rated voltage of WTG	690 VAC
	Rated rotor speed of WTG	10.5 rpm
	Transformer capacity	400 MVA
MAMPC controller	Prediction cycles	15
	Control cycles	3
	Sample time	0.002s

main shaft. To estimate the number of fatigue cycles of the main shaft, the widely used S-N curve method [41] is introduced as shown in (14). S-N curve method can estimate fatigue cycles of the shaft, bearing and blade of WTGs containing metal materials.

$$N = \left[\frac{0.9 \times (2S_u - \tau_{max} - \tau_{min})}{\tau_{max} - \tau_{min}} \right]^m \times 10^3, \qquad (14)$$

where S_u=390 MPa is the yield limit, m is the parameter related to material and load form which is calculated by 3/lg(0.9/k), and k is a constant which reflects the form of mechanical load [41]. $\tau_{\max}$ and $\tau_{\min}$ are obtained by $T_{e,\max}/W_T$ and $T_{e,\min}/W_T$, W_T=21794.8 mm^3 is the torsional section modulus which is obtained according to the structure and material of the main shaft.

IV. SIMULATION AND ANALYSIS

To verify the effectiveness of the proposed techniques, we compare the MAMPC method with the state-of-the-art methods including MMPC, variable droop control and MPPT method. The variable droop control method is set to be proportional to the releasable kinetic energy as shown in (15) [6].

$$K_{droop} = H(\omega_{ri}^2 - \omega_{\min}^2), \qquad (15)$$

Furthermore, an offshore wind farm is modeled in MATLAB. The simulation parameters are shown in Table I.

A. Sudden Load Change

In this case, the 40 WTGs are divided into 4 groups (G1-4) on average at 4 corresponding constant wind speeds of 10, 11, 12 and 13 m/s respectively. Simulation time is set as 15 s. A sudden increase of 0.2 p.u. grid load is set at 5 s to provide a grid frequency variation condition. The corresponding simulation results are shown in Fig. 7.

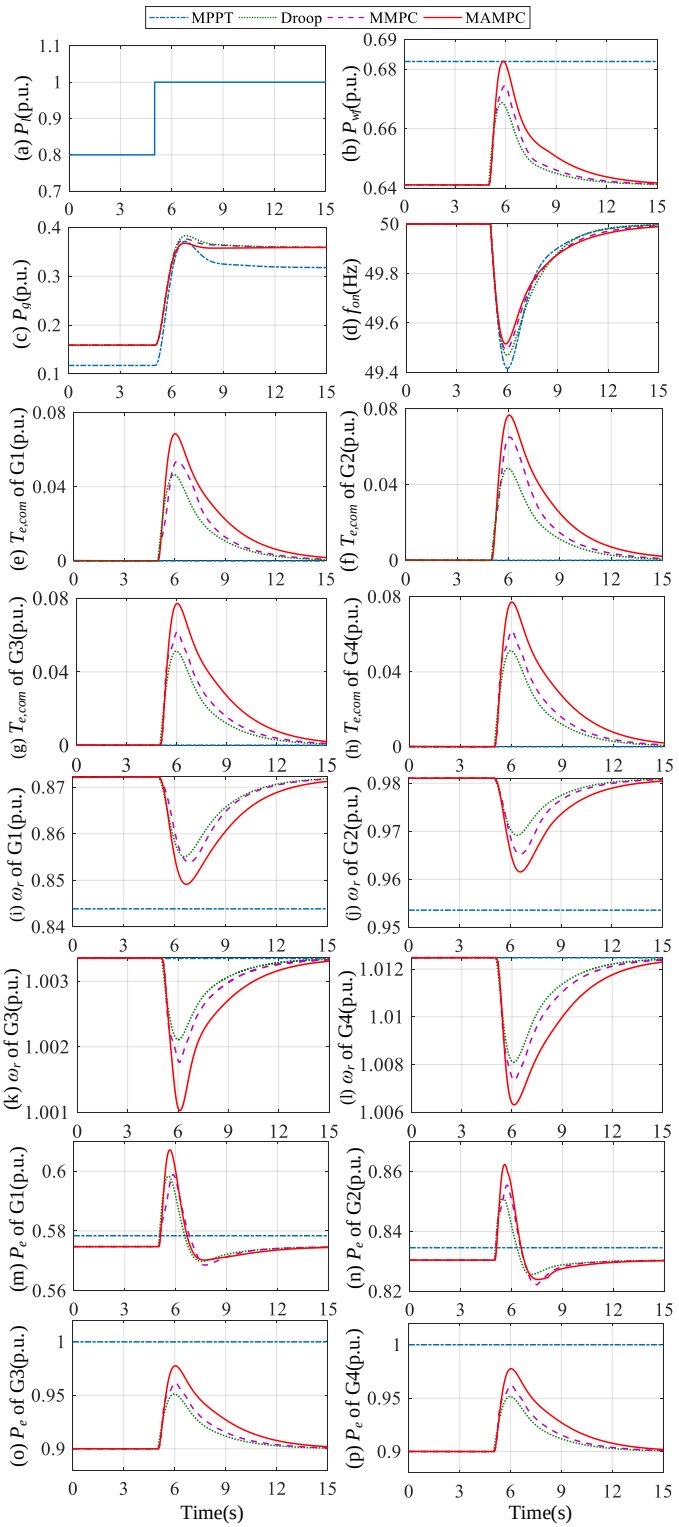

Fig. 7. Simulation results when the load suddenly increases. (a) Load power. (b) Outputs of OWF with different methods. (c) Outputs of AC grid with different methods (power base is 500 MW). (d) AC grid frequency. (e) Torque compensation of WTGs in G1. (f) Torque compensation of WTGs in G2. (g) Torque compensation of WTGs in G3. (h) Torque compensation of WTGs in G4. (i) Rotor speed of WTGs in G1. (j) Rotor speed of WTGs in G2. (k) Rotor speed of WTGs in G3. (l) Rotor speed of WTGs in G4. (m) Power of WTGs in G1. (n) Power of WTGs in G2. (o) Power of WTGs in G3. (p) Power of WTGs in G4, and the power base of WTGs is 8 MW.

In Fig. 7(b), OWF has no available power reserve to support the power shortage under the MPPT control, and its output is constant. The OWF starts to provide power to AC grid when

load power increases at 5 s under the deloading method. In this case, the OWF can quickly provide power to regulate frequency. With the MAMPC, the OWF obtains the real-time operation parameters, and provides more supporting power than other methods. The AC grid experiences the least power change under the MAMPC in Fig. 7(c). The frequency decreases when load increases suddenly in Fig. 7(d). The OWF participates in the frequency suppression. With the MAMPC, the minimum frequency (-0.48Hz) is higher than those with MAMPC (-0.51Hz), variable droop (-0.53Hz) and MPPT(-0.58Hz).

All WTGs compensate torque to regulate their output power. The torque compensation responses to frequency variation of four WTG groups are shown in Figs. 7(e)-(h). Since the power reserves of G3 and G4 are larger than those of G1 and G2, the higher torque of G3 and G4 is compensated. With MAMPC, torque compensations of the individual group are higher than those with the other two frequency regulation methods. Rotor speed of the four groups is shown in Figs. 7(i)-(l). According to the rotor speed, G1-4 are detected in section 1, section 2, section 3 and section 3, respectively. The rotor speed with different frequency regulation methods is declined at different levels due to their corresponding torque compensations. Rotor speed of WTGs is changed, but the influences on the mechanical load are acceptable in this load changing case. Figs. 7(m)-(p) shows the outputs of the individual WTG group. The WTGs with the MAMPC make the largest contribution to power output. At underrated wind speed in Figs. 7(m) and (n), as the WTGs with the frequency regulation methods can use their power reserve and inertia, their peak outputs are higher than those with MPPT for a short time. At overrated wind speed in Figs. 7(o) and (p), their power reserves are utilized to regulate frequency.

B. Wind Speed Change

In this study, to verify the effectiveness of the proposed controllers, the turbulent wind generated by TurbSim is applied for 40 WTGs. Simulation time is set as 120 s. The original wind speed and the filtered wind speed are shown in Fig. 8. The filtered wind speed is obtained by (13). The load power is constant. The simulation results are shown in Fig. 9.

In Fig. 9(a), severe wind speed changes lead to variations of the output power of OWF. In the period of overrated speed, the output power is constant. The variation phenomenon of output power occurs in the period of underrated speed. The change of the OWF output power with MAMPC is the least. Fig. 9(b) shows the output power of AC grid using different methods. Due to the maximum output power of wind farm, the total output power of AC grid using MPPT is lower than those using regulation methods. However, its power change is the largest, which challenges the AC grid frequency regulation capacity. The power change of AC grid with MAMPC is the smoothest due to the corresponding torque compensation. Fig. 9(c) shows the frequency variations. The frequency deviation is the least in all peak and valley points. At the period of underrated wind speed, since the power reserves are limited, the power response contributions and frequency deviation are not enhanced greatly.

In Fig. 9(d), with the MMPC, the frequent torque compensation may lead to the fatigue of mechanical shaft, which challenges the fatigue life of WTG. Although the change rate of torque compensation with variable droop is small, the frequency response capability of wind farm is limited. As for the MAMPC, due to its adaptive ability to the varying operation parameters, the frequency responsibility is enhanced, and the fatigue of main shaft is also mitigated. The rotor speed is shown in Fig. 9(e). The differences in speed with frequency regulation methods are similar because of the huge inertia of WTGs. The torque curves are shown in Fig. 9(f). Furthermore, the S-N curve method is used to estimate the number of fatigue cycles of WTGs under different methods. $T_{e,\max}$ and $T_{e,\min}$ are shown in Fig. 9(f). The estimation results are shown in Table II. It can be seen that comparing with MPPT, the number of fatigue cycles of WTG is extended by the deloading method and torque compensation, and the maximum is 4.58×10^6 with MAMPC.

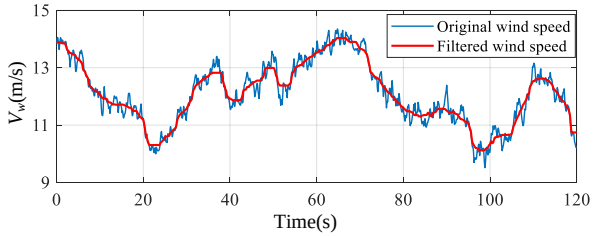

Fig. 8. Original wind speed and filtered wind speed.

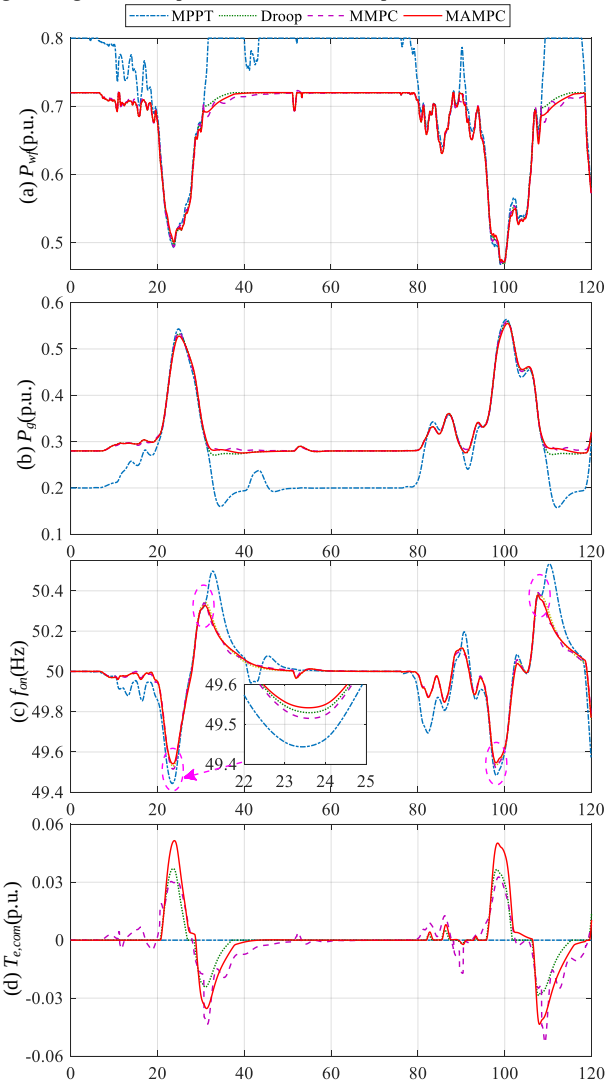

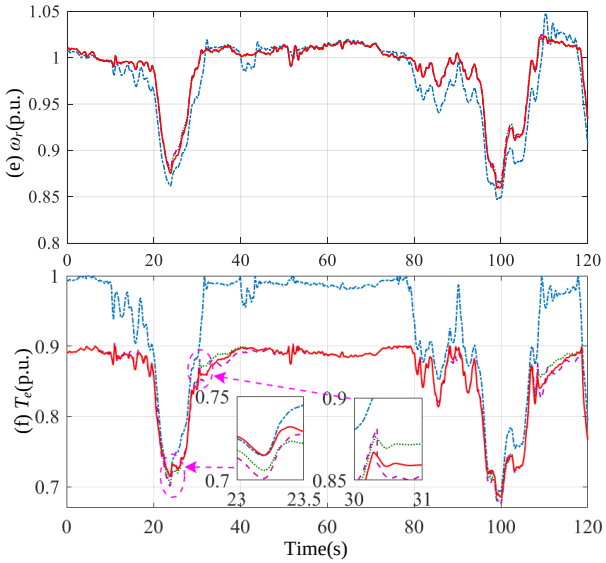

Fig. 9. Simulation results when wind speed increases. (a) Output of OWF with different methods (power base is 500 MW). (b) Output of AC grid with different methods (power base is 500 MW). (c) AC grid frequency. (d) Torque compensation of WTGs. (e) Rotor speed of WTGs. (f) Torque of WTGs.

TABLE II
NUMBER OF FATIGUE CYCLES ESTIMATION RESULTS

Methods	MPPT	Droop	MMPC	MAMPC
τ_{max}(MPa)	348	307.2	309	302.6
τ_{min}(MPa)	250.6	247.5	245.7	250.6
N	2.33×10^4	1.72×10^6	1.22×10^6	4.18×10^6

C. *Long-term Actual Wind Speed*

To further verify the effectiveness of the proposed controllers, comprehensive simulations have been done considering actual wind speeds within one hour and a dynamic load curve. The wind speeds are measured from an actual wind farm, and the load power curve is acquired from State Grid Corporation of China, as shown in Fig. 10. The actual wind speeds are applied for 40 WTGs. Simulation time is set as one hour. The simulation results are shown in Fig. 11.

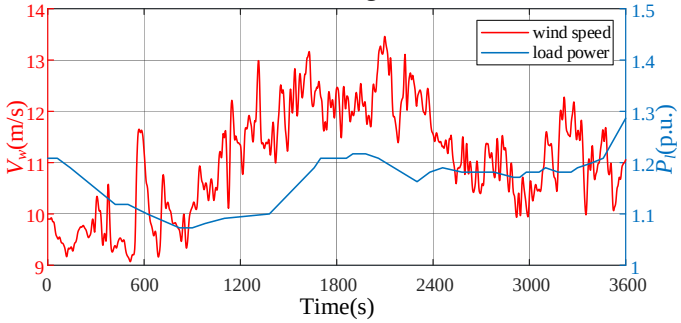

Fig. 10. Actual wind speed and load power curves.

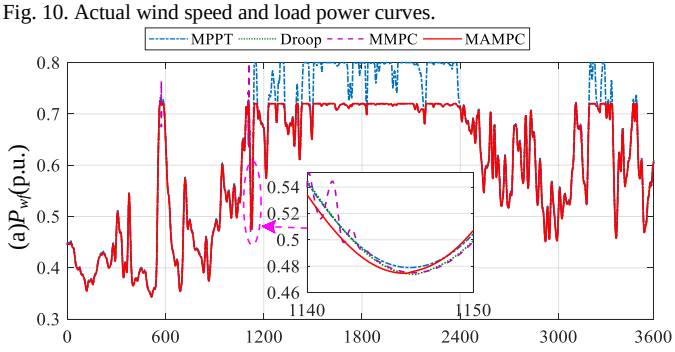

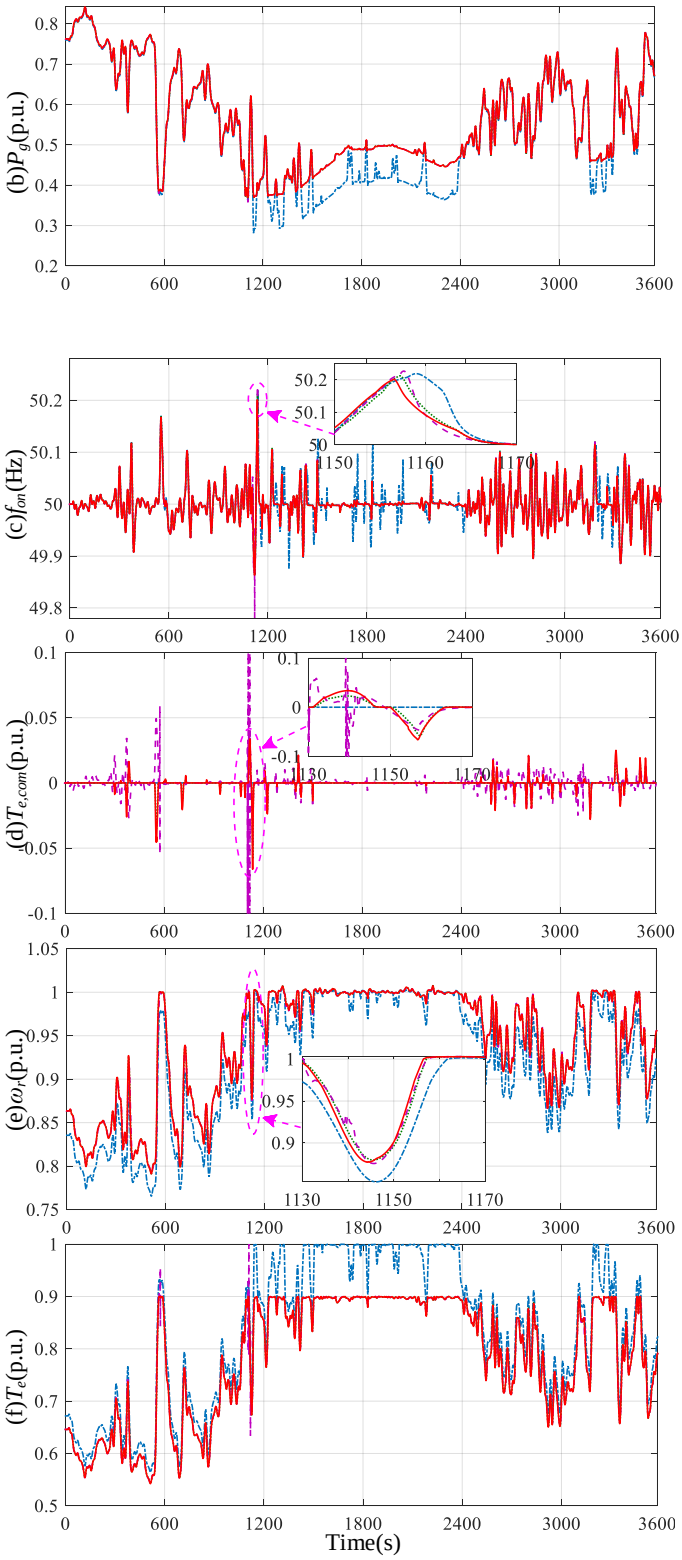

Fig. 11. Simulation results under long-term actual wind speed and dynamic load. (a) Output of OWF with different methods. (b) Output of AC grid with different methods. (c) AC grid frequency. (d) Torque compensation of WTGs. (e) Rotor speed of WTGs. (f) Torque of WTGs.

In Fig. 11(a), the wind speed changes lead to variations of the output power of the OWF and frequency. It can be observed the output power with MPPT is larger than others. To suppress the changes of OWF output and frequency, the WTGs with additional frequency controllers regulate the electric torque and

output power. Compared with MAMPC, the output change of OWF with MMPC is slightly fluctuated, and the valley output with the droop method is enhanced by 0.001 p.u. around t = 1130 s. One may think this value is not large enough. However, all WTGs in power system have the same character, the frequency stability will then be enhanced greatly. Fig. 11(b) shows the output of the AC grid under different methods. Since the output power of OWF using MPPT is the maximum, the total output power of AC grid using MPPT is lower than those using other control methods. Fig. 11(c) shows the frequency variations of AC grid. It can be seen that, during the period of overrated wind speeds, the variation of frequency is relatively less. Compared with the MPPT, droop and MMPC methods, the peak frequency with the proposed is reduced by 0.02 Hz, 0.025 Hz and 0.01 Hz, respectively.

In Fig. 11(d), due to the shortage of parameter estimation, the torque compensation using MMPC is unstable. The response contributions under MAMPC are higher than the variable droop method. The rotor speed is shown in Fig. 11(e). The differences in speed with different frequency regulation methods are similar thanks to the huge inertia of WTGs. Fig. 11(f) shows the torque curves.

V. Conclusion

This paper proposes a multiple adaptive model predictive controller (MAMPC), which seamlessly integrates the multiple model predictive control and the real-time ARX model. The proposed MAMPC technique can predict the WTG operating parameters by ARX models and restrict the rate of change in torque compensation. The specific conclusions are as follows.

- The MAMPC improves the frequency response capability and mitigates the main shaft mechanical load in all of the speed sections, which is applicable to the deloaded wind farm.
- Comparing with the state-of-the-art techniques of MPPT, variable droop and MMPC, the minimum frequency deviation with the proposed method is reduced by 0.1 Hz, 0.05 Hz and 0.03 Hz, respectively in the case of a 0.2 p.u. grid load rise.
- The estimated number of fatigue cycles that main shaft can be suffered, is also extended by 4.15×10^6, 2.46×10^6, 2.96×10^6 cycles in the case of turbulent wind, respectively.

In the furfure work, we will consider the tower shadow and torque ripple at 3 times the rotational frequency of blades in the fatigue estimator.

References

[1] Y. Liu, S. Hu and A. Y. Zomaya, "The hierarchical smart home cyberattack detection considering power overloading and frequency disturbance," *IEEE Trans. Ind. Informat.*, vol. 12, no. 5, pp. 1973-1983, 2016.

[2] Gopal Singh and Kalpathy Sundaram, "Methods to improve wind turbine generator bearing temperature imbalance for onshore wind turbines," *Wind Engineering*, vol. 46, no. 1, pp. 150-159, 2022.

[3] Gopal Singh, Kalpathy Sundaram and Marco Matuonto, "A solution to reduce overheating and increase wind turbine systems availability," *Wind Engineering*, vol. 45, no. 3, pp. 491-504, 2021.

[4] A. Attya, J. Dominguez-Garcia and O. Anaya-Lara, "A review on frequency support provision by wind power plants: current and future challenges," *Renewable and Sustainable Energy Reviews*, vol. 81, pp. 2071-2087, 2018.

[5] Y. Wu, Y. Hu and W. Hsu, "Inertial support from WPPs that include VSWTs – a review," *The Journal of Engineering*, vol. 2019, no. 7, pp. 4633-4643, 2019.

[6] J. Lee, G. Jang, E. Muljadi, F. Blaabjerg, Z. Chen and Y. C. Kang, "Stable short-term frequency support using adaptive gains for a DFIG-based wind power plant," *IEEE Trans. Energy Convers.*, vol. 31, no. 3, pp. 1068-1079, 2016.

[7] T. L. Van, T. H. Nguyen and D. C. Lee, "Advanced pitch angle control based on fuzzy logic for variable-speed wind turbine systems," *IEEE Trans. Energy Convers.*, vol. 30, no. 2, pp. 578-587, 2015.

[8] F. Wilches-Bernal, J. H. Chow and J. J. Sanchez-Gasca, "A fundamental study of applying wind turbines for power system frequency control," *IEEE Trans. Power Syst.*, vol. 31, no. 2, pp. 1496-1505, 2016.

[9] U. Datta, J. Shi and A. Kalam, "Primary frequency control of a microgrid with integrated dynamic sectional droop and fuzzy based pitch angle control," *Electrical Power and Energy Systems*, vol. 111, pp. 248-259, 2019.

[10] S. Wang and K. Tomsovic, "A novel active power control framework for wind turbine generators to improve frequency response," *IEEE Trans. Power Syst.*, vol. 33, no. 6, pp. 6579-6589, 2018.

[11] H. Wang, J. Yang, Z. Chen, W. Ge, S. Hu, Y. Ma, Y. Li, G. Zhang and L. Yang, "Gain scheduled torque compensation of PMSG-based wind turbine for frequency regulation in an isolated grid," *Energies*, vol. 11, no. 7, p. 1623, 2018.

[12] H. Luo, Z. Hu, H. Zhang and H. Chen, "Coordinated active power control strategy for deloaded wind turbines to improve regulation performance in AGC," *IEEE Trans. Power Syst.*, vol. 34, no. 1, pp. 98-108, 2019.

[13] L. Shang, J. Hu, X. Yuan and Y. Chi, "Understanding inertial response of variable-speed wind turbines by defined internal potential vector," *Energies*, vol. 10, no. 1, p. 22, 2017.

[14] Z. Wu, W. Gao, T. Gao, W. Yan, H. Zhang, S. Yan and X. Wang, "State-of-the-art review on frequency response of wind power plants in power systems," *Journal of Modern Power Systems and Clean Energy*, vol. 6, no. 1, pp. 1-16, 2018.

[15] M. F. M. Arani and Y. A.-R. I. Mohamed, "Dynamic droop control for wind turbines participating in primary frequency regulation in microgrids," *IEEE Trans. Smart Grid*, vol. 9, no. 6, pp. 5742-5751, 2018.

[16] T. T. Nguyen, H. J. Yoo and H. M. Kim, "A droop frequency control for maintaining different frequency qualities in a stand-alone multimicrogrid system," *IEEE Trans. Sustain. Energy*, vol. 9, no. 2, pp. 599-609, 2018.

[17] T. Liu, W. Pan, R. Quan and M. Liu, "A variable droop frequency control strategy for wind farms that considers optimal rotor kinetic energy," *IEEE Access*, vol. 7, pp. 68636-68645, 2019.

[18] G. Li, J. Liang, F. Ma, C. E. Ugalde-Loo and H. Liang, "Analysis of single-phase-to-ground faults at the valve side of HB-MMC in HVDC converter stations," *IEEE Trans. Ind. Electron.,* vol. 66, no. 3, pp. 2444-2453, March 2019.

[19] J. N. Sakamuri, M. Altin, A. D. Hansen and N. A. Cutululis, "Coordinated frequency control from offshore wind power plants connected to multi terminal DC system considering wind speed variation," *IET Renewable Power Generation*, vol. 11, no. 8, pp. 1226-1236, 2017.

[20] H. Ye, W. Pei, L. Kong and T. An, "Low-order response modeling for wind farm-MTDC participating in primary frequency controls," *IEEE Trans. Power Syst.*, vol. 34, no. 2, pp. 942-952, 2019.

[21] F. D. Bianchi and J. L. Domínguez-García, "Coordinated frequency control using MT-HVDC grids with wind power plants," *IEEE Trans. Sustain. Energy*, vol. 7, no. 1, pp. 213-220, 2016.

[22] O. D. Adeuyi, M. Cheah-Mane, J. Liang and N. Jenkins, "Fast frequency response from offshore multiterminal VSC–HVDC schemes," *IEEE Trans. Power Del.*, vol. 32, no. 6, pp. 2442-2452, 2017.

[23] K. Jose, T. Joseph, J. Liang and C. E. Ugalde-Loo, "Auxiliary dead-band controller for the coordination of fast frequency support from multi-terminal HVDC grids and offshore wind farms," *IET Renewable Power Generation*, vol. 12, no. 13, pp. 1444-1452, 2018.

[24] R. You, B. Barahona, J. Chai and N. A. Cutululis, "Frequency support capability of variable speed wind turbine based on electromagnetic coupler," *Renewable Energy*, vol. 74, pp. 681-688, 2015.

[25] M. F. M. Arani and Y. A. I. Mohamed. "Analysis and damping of mechanical resonance of wind power generators contributing to frequency regulation,". *IEEE Trans. Power Syst.*, vol. 12, no. 4, pp. 3195-3204, 2017.

[26] X. Xi, H. Geng, G. Yang, S. Li and F. Gao, "Torsional oscillation damping control for DFIG-based wind farm participating in power system frequency regulation," *IEEE Trans. Ind. Appl.*, vol. 54, no. 4, pp. 3687-3701, 2018.

[27] R. You, B. Barahona, J. Chai, N. A. Cutululis and X. Wu, "Improvement of grid frequency dynamic characteristic with novel wind turbine based on electromagnetic coupler," *Renewable Energy*, vol. 113, pp. 813-821, 2017.

[28] Q. Yao, J. Liu, Y. Hu. "Optimized active power dispatching strategy considering fatigue load of wind turbines during de-loading operation," *IEEE Access*, vol. 7, pp. 17439-17449, 2019.

[29] L. Huang, F. Chen, H. Yuan, Z. Lan, H. Xin and Z. Wang, "Frequency support from kinetic energy of DFIG-based wind turbines considering speed limitation," in *Proceedings of the IEEE PES General Meeting, Atlanta*, GA, USA, 2019, pp. 1-5.

[30] M. Kang, K. Kim, E. Muljadi, J. W. Park and Y. C. Kang, "Frequency control support of a doubly-fed induction generator based on the torque limit," *IEEE Trans. Power Syst.*, vol. 31, no. 6, pp. 4575-4583, 2016.

[31] X. Liu, Y. Zhang and K. Y. Lee, "Coordinated distributed MPC for load frequency control of power system with wind farms," *IEEE Trans. Ind. Informat.*, vol. 64, no. 6, pp. 5140-5150, 2017.

[32] M. Ma, C. Zhang, X. Liu and H. Chen, "Distributed model predictive load frequency control of the multi-area power system after deregulation," *IEEE Trans. Ind. Electron.*, vol. 64, no. 6, pp. 5219-5139, 2017.

[33] H. Wang, J. Yang, Z. Chen, W. Ge, Y. Ma, Z. Xing and L. Yang, "Model predictive control of PMSG-based wind turbines for frequency regulation in an isolated grid," *IEEE Trans. Ind. Appl.*, vol. 54, no. 4, pp. 3077-3089, 2018.

[34] Z. Song, F. Zhou and Z. Zhang, "Parallel-observer-based predictive current control of permanent magnet synchronous machines with reduced switching frequency," *IEEE Trans. Ind. Informat.*, vol. 12, no. 12, pp. 6457-6467, 2019.

[35] Z. Song and F. Zhou, "Observer-based predictive vector-resonant current control of permanent magnet synchronous machines," *IEEE Trans. Power Electron.*, vol. 34, no. 6, pp. 5969-5980, 2019.

[36] S. Ebadollahi and S. Saki, "Wind turbine torque oscillation reduction using soft switching multiple model predictive control based on the gap metric and kalman filter estimator," *IEEE Trans. Ind. Electron.,* vol. 65, no. 5, pp. 3890-3898, 2018.

[37] A. S. Mir and N. Senroy, "Adaptive model predictive control scheme for application of SMES for load frequency control," *IEEE Trans. Power Syst.*, 2020. (Early Access)

[38] Z. Lu, Y. Ye and Y. Qiao, "An adaptive frequency regulation method with grid-friendly restoration for VSC-HVDC integrated offshore wind farms," *IEEE Trans. Power Syst.*, vol. 34, no. 5, pp. 3582-3593, 2019.

[39] S. Zhan, J. Na, G. Li and B. Wang, "Adaptive model predictive control of wave energy converters," *IEEE Trans. Sustain. Energy*, vol. 11, no. 1, pp. 229-238, 2020.

[40] P. Mattias and P. Chen, "Frequency control by variable speed wind turbines in islanded power systems with various generation mix," *IET Renewable Power Generation,* vol. 11, no. 7, pp. 1101-1109, 2017.

[41] K. Tian, P. Wang, W. Qin, X. Han, Y. Jia and C. Liang, "Fatigue reliability analysis of wind turbines shafts caused by sub-synchronous oscillations during power system fault," in *Proceedings of the International Conference on Probabilistic Methods Applied to Power Systems (PMAPS)*, Beijing, China 2016, pp. 1-6.

Haixin Wang received the B.Eng. degree in electrical engineering from the Inner Mongolia Agricultural University, Hohhot, China, in 2011, and the M.Sc. and Ph.D. degrees in electrical engineering from the Shenyang University of Technology, Shenyang, China, in 2014 and 2017, respectively. He did his postdoctoral research at the Shenyang University of Technology, Shenyang, China, and at school of engineering, Cardiff University, Cardiff, UK, in 2018 and 2019. Currently, He is an associate professor at School of Electrical Engineering, Shenyang University of Technology, Shenyang, China. His research interests include integrated energy system, wind power generation and cyber-physical system.

Zihao Yang got his B.S. degree in Automation from Northeastern University, Shenyang, China, in 2015; M.S degree in Electrical and Computer Engineering from University of Illinois at Chicago, Chicago, America, in 2017. Now he is a PhD student at School of Electrical Engineering, Shenyang University of Technology, Shenyang, China. His current research interests major on digital twin, cyber-phsical system and wind power generation.

Zhe Chen (M'95-SM'98-F'19) received the B.Eng. and M.Sc. degrees from the Northeast China Institute of Electric Power Engineering, Jilin City, China, in 1982 and 1986, and the Ph.D. degree from the University of Durham, U.K., in 1997. Dr. Chen is a Full Professor with the Department of Energy Technology, Aalborg University, Denmark. He is the Leader of Wind Power System Research program at the Department of Energy Technology, Aalborg University and the Danish Principle Investigator for Wind Energy of Sino-Danish Centre for Education and Research. His research areas are power systems, power electronics and electric machines, and his main current research interests are wind energy and modern power systems. He has led many research projects and has more than 500 publications in his technical fields.

Jun Liang (M'02-SM'12) received the B.Sc. degree in Electric Power System & its Automation from Huazhong University of Science and Technology, Wuhan, China, in 1992 and the M.Sc. and Ph.D. degrees in Electric Power System & its Automation from the China Electric Power Research Institute (CEPRI), Beijing, in 1995 and 1998, respectively.

From 1998 to 2001, he was a Senior Engineer with CEPRI. From 2001 to 2005, he was a Research Associate with Imperial College London, U.K. From 2005 to 2007, he was with the University of Glamorgan as a Senior Lecturer. He is currently a Professor in Power Electronics with the School of Engineering, Cardiff University, Cardiff, U.K. He is the Coordinator and Scientist-in-Charge of two European Commission Marie-Curie Action ITN/ETN projects: MEDOW (€3.9M) and InnoDC (€3.9M). His research interests include HVDC, MVDC, FACTS, power system stability control, power electronics, and renewable power generation.

Prof. Liang is a Fellow of the Institution of Engineering and Technology (IET). He is the Chair of IEEE UK and Ireland Power Electronics Chapter. He is an Associate Editor-in-Chief of CSEE JPES. He is an Editor of the IEEE Transactions on Sustainable Energy.

Gen Li (M'18) received the B.Eng. degree in Electrical Engineering from Northeast Electric Power University, Jilin, China, in 2011, the M.Sc. degree in Power Engineering from Nanyang Technological University, Singapore, in 2013 and the Ph.D. degree in Electrical Engineering from Cardiff University, Cardiff, U.K., in 2018.

He is now an Associate Professor in Power System Protection at Technical University of Denmark (DTU), Ballerup, Denmark. From 2013 to 2016, he was a Marie Curie Early Stage Research Fellow funded by the European Commission's MEDOW project. He has been a Visiting Researcher at China Electric Power Research Institute and Global Energy Interconnection Research Institute, Beijing, China, at Elia, Brussels, Belgium and at Toshiba International (Europe), London, U.K. He was a Research Associate at the School of Engineering, Cardiff University from 2018 to 2022. His research interests include control and protection of HVDC and MVDC technologies, power electronics, reliability modelling and evaluation of power electronics systems.

Dr. Li is a Chartered Engineer in the U.K. He is an Associate Editor of the CSEE Journal of Power and Energy Systems. He is an Editorial Board Member of CIGRE ELECTRA. He is an IET Professional Registration Advisor. His Ph.D. thesis received the First CIGRE Thesis Award in 2018. He is the Vice-Chair of IEEE PES Young Professionals and the Technical Panel Sectary of CIGRE UK B5 Protection and Automation.

Junyou Yang received the B.Eng. degree from Jilin University of Technology, Jilin City, China, the M.Sc. degree from Shenyang University of Technology, Shenyang, China, and the Ph.D. degree from Harbin Institute of Technology, Harbin, China. He was a Visiting Scholar at Department of Electrical Engineering and Computer Science, University of Toronto, Canada, from 1999 to 2000. He is the Head of School of Electrical Engineering, Shenyang University of Technology, Shenyang, China. He is a Distinguished Professor of Liaoning province and the first hundred level candidates in "BaiQianWan Talents Program". He has led more than fifty research projects and has more than 200 publications in his technical field. His research interests include wind energy, power system and integrated energy system.

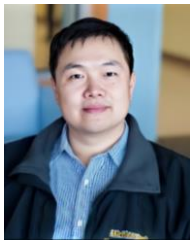

Shiyan Hu (SM'10) received his Ph.D. in Computer Engineering from Texas A&M University in 2008. He is the Professor and Chair in Cyber-Physical System Security at University of Southampton. His research interests include Cyber-Physical Systems and Cyber-Physical System Security, where he has published more than 150 refereed papers. He is an ACM Distinguished Speaker, an IEEE Systems Council Distinguished Lecturer, a recipient of the 2017 IEEE Computer Society TCSC Middle Career Researcher Award, and a recipient of the 2014 U.S. National Science Foundation (NSF) CAREER Award. His publications have received a few distinctions such as the 2018 IEEE Systems Journal Best Paper Award, the 2017 Keynote Paper in IEEE Transactions on Computer-Aided Design, the Front Cover Paper in IEEE Transactions on Nanobioscience in March 2014, etc. He is the Chair for IEEE Technical Committee on Cyber-Physical Systems. He is the Editor-In-Chief of IET Cyber-Physical Systems: Theory & Applications. He is an Associate Editor for IEEE Transactions on Computer-Aided Design, IEEE Transactions on Industrial Informatics, IEEE Transactions on Circuits and Systems, ACM Transactions on Design Automation for Electronic Systems, and ACM Transactions on Cyber-Physical Systems. He is also a Guest Editor for eight IEEE/ACM journals such as Proceedings of the IEEE and IEEE Transactions on Computers. He has held chair positions in various IEEE/ACM conferences. He is a Member of European Academy of Sciences and Arts, a Fellow of IET, and a Fellow of British Computer Society.